galaxies

MDPI

Article

Unraveling the Physics of Quasar Jets: Optical Polarimetry and Implications for the X-ray Emission Process

Eric S. Perlman [1,†], Devon Clautice [1,†], Sayali Avachat [1,*,†] Mihai Cara [2,*] William B. Sparks [2,*], Markos Georganopoulos [2,*] and Eileen Meyer [3,*]

1 Department of Physics and Space Sciences, Florida Institute of Technology, Melbourne, FL 32901, USA; eperlman@fit.edu (E.S.P.); dclautice2012@my.fit.edu (D.C.)
2 Space Telescope Science Institute, Space Telescope Science Institute, Mountain View, CA 94043, USA
3 Department of Physics, University of Maryland, Baltimore, MD 21250, USA
* Correspondence: ssavachat@gmail.com (S.A.); mcara@stsci.edu (M.C.); wsparks@seti.org (W.B.S.); georgano@umbc.edu (M.G.); meyer@umbc.edu (E.M.)
† These authors contributed equally to this work.

Received: 25 March 2020; Accepted: 28 August 2020; Published: 27 September 2020

Abstract: Since the launch of Chandra twenty years ago, one of the greatest mysteries surrounding Quasar Jets is the production mechanism for their extremely high X-ray luminosity. Two mechanisms have been proposed. In the first view, the X-ray emission is inverse-Comptonized CMB photons. This view requires a jet that is highly relativistic (bulk Lorentz factor >20–40) on scales of hundreds of kiloparsecs, and a jet that is comparably or more powerful than the black hole's Eddington luminosity. The second possibility is synchrotron emission from a high-energy population of electrons. This requires a much less powerful jet that does not need to be relativistically beamed, but it imposes other extreme requirements, namely the need to accelerate particles to >100 TeV energies at distances of hundreds of kiloparsecs from the active nucleus. We are exploring these questions using a suite of observations from a diverse group of telescopes, including the *Hubble Space Telescope (HST)*, *Chandra* X-ray Observatory *(CXO)*, *Fermi* Gamma-ray Space Telescope and various radio telescope arrays. Our results strongly favor the hypothesis that the X-ray emission is synchrotron radiation from a separate, high-energy electron population. We discuss the observations, results and new questions brought up by these surprising results. We investigate the physical processes and magnetic field structure that may help to accelerate particles to such extreme energies.

Keywords: galaxies: active; galaxies: jets; quasars: individual: 3C 273; quasars: individual: PKS 0637-752; quasars: individual; 1150+497

1. Introduction

Quasar jets carry energy and matter out from the nucleus to $>$ 100 kpc scale lobes. Emerging from the central parsec of their host galaxy, they can effectively transform the galaxy on a broad scale and with it, the cluster they sit in. While found in only $\sim$ 10% of active galactic nuclei (AGN), jets can have a power output comparable to that of the host galaxy [1]. High-power, FR II radio jets typically terminate in bright "hot-spots" and are very straight and edge-brightened, while lower-power, FR I sources are brightest at the core and edge-dimmed [2].

In low-power Fanaroff–Riley Class I (FR I) radio galaxies [2], the radio fluxes and spectra can usually be extrapolated and predict well the optical and X-ray fluxes (see, e.g., [3–5]). This and high optical polarizations (typically $\sim$ 20–30%, [6,7]) suggest synchrotron emission up to at least X-ray energies. The polarization properties [7–10] are often correlated with X-ray emission.

For example, in the knots of the jet of M87 [5], we found an anti-correlation between X-ray emission and optical polarization, along with changes in the magnetic field direction. This suggested a link between the jet's dynamical structure and high-energy emission processes within the jet interior, which we suggested was where shocks compress the magnetic field and particles were accelerated.

For the more powerful Fanaroff–Riley Class II (FR II, [2]) and quasar jets, the nature of the optical and X-ray emission is unclear. The reason for this is that in many objects, the optical emission can lie well below a power-law interpolation of the radio-to-X-ray SED, using only the spectral index α_{RX} ($F_\nu \propto \nu^{-\alpha_{RX}}$), e.g., [11]—by decades in the case of PKS 0637–752 [12,13]. This results in a double-humped spectral energy distribution (SED). In some jets, such as 3C 273 and PKS 1136–135 [14–18], the optical emission appears linked to the X-ray emission by a common component that is distinct from the lower-energy synchrotron emission. This component is first seen at near-IR/optical energies and dominates the jet SED in the UV to X-rays, extending up to at least 10 keV.

Two competing mechanisms have been proposed for the origin of the X-ray emission. The first possibility is synchrotron radiation from very high-energy electrons, arising in a component separate from the lower-energy, radio to optical emission. This mechanism, discussed in detail by [19], requires an electron energy distribution that can extend up to hundreds of TeV and in situ particle acceleration, and imposes much lower energetic demands on the jet. The second, competing mechanism, is inverse-Comptonization of low-energy photons by relativistic electrons within the jet see [19,20]. Moreover, the origin of the seed photons cannot be constrained by multi-waveband spectra alone [21].

As synchrotron emission is naturally polarized, polarization can be a powerful diagnostic of jet emission processes. High polarization indicates a highly ordered magnetic field, and the inferred direction of the magnetic field vector indicates the flux-weighted direction of the magnetic field in the radiating volume, modulo relativistic aberration. The existence of such a component would drastically alter our picture of FR II jets, requiring efficient particle acceleration mechanisms tens to hundreds of kpc outside the host galaxy [22] and without evidence of a dynamically obvious feature such as a terminal shock or bend. For this reason, it was originally thought to be implausible to explain the X-ray emission from the kiloparsec-scale jets as synchrotron emission, although it was first raised as a possible alternative to the IC-CMB model by [22]. Physically, there is no real reason why this mechanism, which is responsible for the X-ray emission in FR I radio galaxies (e.g., [4,5]) cannot operate in FR II jets as well. Optical-to-X-ray synchrotron radiation predicts optical polarization that is high, comparable to that seen in the radio, but reflecting a different emitting volume in its position angle characteristics, as seen in several papers for FR I jets [6–10,23], where the optical jet emissions reflect a much more short-lived (100–1000 years) radiating electron population than that in the radio (where the typical particle lifetime can be millions of years).

Two other emission mechanisms are possible. The first is synchrotron self-Compton (SSC) emission, where the seed photons are at meter-wavelengths or longer, and come from within the jet. SSC is unavoidable is unlikely to dominate the knot X-ray emission because it requires the jet to either be massively out of equipartition (by factors of 20–100), or be viewed at nearly 90° (see, e.g., [24]). That might be the case to explain the kiloparsec-scale X-ray emission of a few FR II jets, but it cannot explain the X-ray emission of the larger population. However, SSC is the leading scenario for X-ray emission from the terminal hotspots of powerful jets [25,26].

The final candidate process, which dominated the discussion for over a decade, is inverse-Comptonization of photons from the cosmic microwave background (IC-CMB) [27]. This requires a jet that is highly relativistic, even hundreds of kpc out from the AGN [12,28,29], that is viewed within a few degrees of its beaming axis. Any optical IC-CMB would be linked to electrons with $\gamma < 10$, a heretofore-untracked particle population. If detected, these particles would carry the lion's share of the jet's matter content and energy budget (e.g., [30]). If the emitter has bulk $\Gamma \gg 1$ then the forward-bunching effect of special relativity would make CMB photons essentially unidirectional in the jet frame, causing them to be unpolarized when upscattered by ultra-relativistic electrons. On the other hand, radiation scattered radiation by cold electrons ($\gamma \sim 1$; so-called Bulk

Comptonization) should be highly polarized [31]. Krawczynski [32] carried out calculations covering the intermediate regime with $\gamma \sim$ few. In this regime, they found a degree of polarization as large as 8% with the direction of the electric field vector perpendicular to the jet axis see also [33]. Thus the degree of polarization and direction of polarization of optical jet emission represents a very interesting test of jet emission mechanisms, as highly polarized optical emission from kiloparsec-scale FR II jets would be strong evidence against the IC-CMB mechanism.

In [34], we discussed *HST* polarimetry observations of PKS 1136–135, a low-polarization quasar which has an optical jet that has an SED where the optical and X-ray emission that are smoothly connected by a single power-law that is inconsistent with the radio emission. Our results revealed a highly polarized jet, with three components that had polarizations in the optical of $\gtrsim 30\%$. As shown in that paper, the IC-CMB interpretation could not explain the observed SED plus polarization characteristics, as they would require an extraordinarily high amount of relativistic beaming ($\Gamma \sim 40$ and $\theta < 3°$), that is inconsistent with other known properties of PKS 1136–135, as a low-polarization quasar that is not violently variable and thus rather unlikely to be so highly beamed. We therefore interpreted its optical and X-ray emission in the context of a second, high-energy synchrotron emission component that required in situ particle acceleration.

More recently, analysis of *Fermi* observations of multiple other quasars [35–38] including the jets of 3C 273 and PKS 0637–752, also proved to be inconsistent with the IC-CMB emission process being dominant in the X-rays, as the same electron population would inverse-Comptonize optical synchrotron photons into the GeV gamma-ray band, thus requiring a similarly high beaming factor that overpredicts the observed low-state emissions detected by *Fermi* by orders of magnitude. While 3C 273 has components with varying apparent speeds, as high as 15*c* (see, e.g., [39]), those components are on parsec scales, while the observed X-ray emission is on projected scales of tens of kiloparsecs, where *HST* observations have failed to find any evidence of superluminal motions [40]. A similar problem exists for PKS 0637–752, where VLBI observations [41] show similarly fast, superluminal components. As there are a variety of strong arguments (see, e.g., [22,42]) that suggest that quasar jets decelerate significantly on kiloparsec scales, such high beaming factors on large scales must be viewed as unlikely at best.

Here we present *HST* polarimetry observations of three additional quasar jets, those of 3C 273 ($z = 0.158$), PKS 0637–752 ($z = 0.653$), and 1150 + 497 ($z = 0.334$). Each of these has a SED remarkably similar to that of PKS 1136–135, albeit with the high-energy emission component beginning at shorter wavelengths than that object—in the optical for 1150 + 497 [43], but in the UV for PKS 0637-752 [13] and 3C 273 [15,16,44]. These observations show optical emissions from multiple components in the jets of all three components that are moderately (10–40%) polarized. These results further bolster the case for synchrotron emission being the dominant mechanism to explain the optical-to-X-ray emission of each of these jets.

2. Methods

The F606W filter was chosen for the following reasons: (i) based on existing data prior to this work, its pivot wavelength falls inside the "dip" between the low-energy (radio to infrared) and the high-energy (optical to X-ray) bumps of the broadband spectrum thus minimizing contribution from the low-energy (synchrotron) component to the total flux and polarization; (ii) it complements existing observations at other optical wavelengths; (iii) it provides the most optimal performance of the POLV filters (i.e., maximized parallel and minimized perpendicular transmissions).

2.1. Polarimetric Observations

We performed optical polarimetry with the Advanced Camera for Surveys (ACS) aboard the *HST* using the wide field camera (WFC) chips, the F606W spectral filter and the POL(0,60,120)V polarizing filter set for all observations. This gave three different polarizer orientations. Total exposure times and observation dates are given in Table 1. We used a simple line-dither pattern for the pointings. Both short

and long exposures were done This allowed for a better recovery of information in defective/hot pixels and pixels affected by cosmic rays (CR) and other defects.

Table 1. Hubble Space Telescope (*HST*) Polarimetry Observations.

Jet	Program	Instrument	Filter Set	Date	Exposure [a] (s)
1150 + 479	11,138	ACS/WFC	F606W + POL(0,60,120)V	19–23 December 2010	7890 [b]
3C 273	13,764	ACS/WFC	F606W + POL(0,60,120)V	6–8 January 2015	5240
PKS 0637–752	14,696	ACS/WFC	F606W + POL(0,60,120)V	17–23 November 2017	11,585

[a] Exposure times are per polarizing filter combination. Total exposure time is a factor three higher. [b] An additional 524 s of exposure time was obtained in the POL120V filter at the end of an orbit.

2.2. Data Reduction

All *HST* images were re-calibrated using up-to-date reference files obtained from the STScI Calibration Database system. Since the *HST* data were taken with the ACS instrument, the ACS Destripe Plus module from the ACSTOOLS Python library was used to correct for instrument artifacts such as CTE degradation and striping. Images were aligned using Tweakreg and combined using Astrodrizzle. The images from each polarizing filter were combined to form the Stokes images using the method prescribed in the ACS Instrument Handbook. We combined the resulting Stokes I, Q, and U images to produce the fractional polarization map $P = \sqrt{Q^2 + U^2}/I$.

For each of the three jets, archival radio data was used for comparison with the optical polarimetry. For PKS 0637–752, archival 8.64 GHz data from the Australia Telescope Compact Array (ATCA) [45] was used. For 1150 + 497, archival 1.66 GHz data from the Multi-Element Radio Linked Interferometer Network (MERLIN) [43] was used. For 3C 273, archival 8.4 GHz VLA data [46] and archival Chandra data [15] were used for comparison. Please see the above papers for details on the observations and data reduction procedures for the comparison data.

2.3. Aperture Polarimetry and Photometry

We measured the fluxes and polarizations of jet regions using several, varying size apertures for each knot. Positions and sizes of the apertures were chosen to avoid nearby saturated columns, diffraction spikes, or other sources. Larger apertures included most of the flux, requiring minimal aperture correction but producing larger Poisson errors in flux and polarization due to the inclusion of many low S/N pixels. On the other hand, smaller apertures produced higher S/N, but require much larger aperture corrections. Then, for any region k, the flux and polarization are computed as weighted means:

$$I = \sum_k I_k/\sigma_k^2 \tag{1}$$

with an error estimate given by:

$$\sigma_I = \left(\sum_k 1/\sigma_k^2\right)^{-1/2}, \tag{2}$$

where we sum over apertures of different sizes.

3. Results

Each of the jets we observed in this work—3C 273 (Figure 1), PKS 0637–752 (Figure 2) and 1150+497 (Figure 3)—show moderately to highly polarized components. All three have multiple discrete emission sites with 10–40% polarization, and 3C 273 also has significant polarization seen in locations outside of knots. Particularly notable are eight regions in the 3C 273 jet that are at the jet edges and/or in interknot regions. The fractional polarization for these regions (circled in Figure 3) all range from 10–30%, and in every case, the nearest knot maximum has a significantly lower polarization.

A similar behavior was seen by [34] for PKS 1136–135, but in 3C 273 we have many more regions and a factor two better physical resolution.

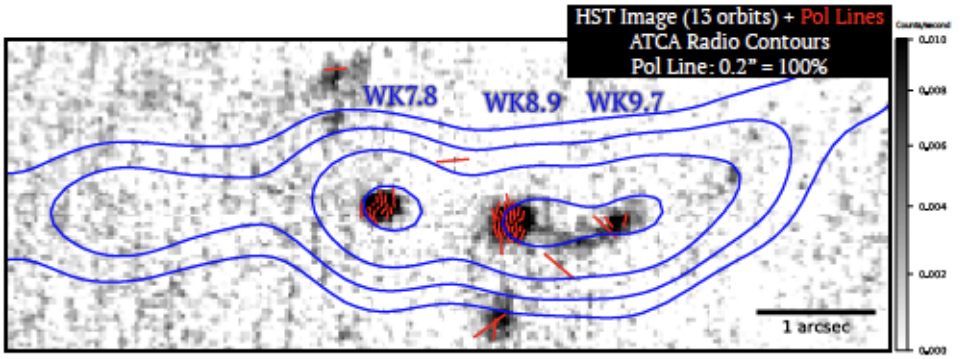

Figure 1. Optical (*HST*/ACS + F606W) Stokes I image of the jet of PKS 0637–752 is shown, with radio 8.64 GHz contours from Australia Telescope Compact Array (ATCA) observations in blue and optical polarization E-vectors in red. We have filtered polarization vectors by showing only pixels with optical polarization SNR > 3.0. Polarization vectors are of scale 0.2 arcsec = 100% polarization. Radio contours increase by factors of two. Three polarized jet regions are seen, with other regions falling below the detection limit. Polarizations are as high as 31%. The greyscale is at far right. See text for details.

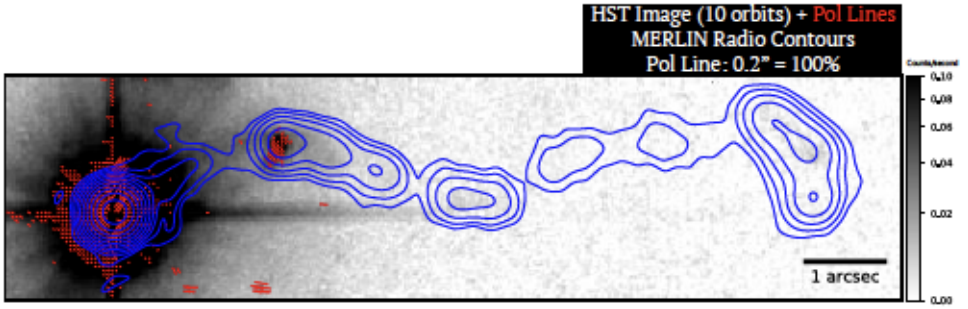

Figure 2. Optical (*HST*/ACS + F606W) Stokes I image of the nucleus and jet of 1150+497 is shown, with radio 1.66 GHz contours from Multi-Element Radio Linked Interferometer Network (MERLIN) observations in blue and optical polarization E-field vectors overlaid in red. We have filtered polarization vectors by showing only pixels with optical polarization SNR > 4.0. Polarization vectors are of scale 0.2 arcsec = 100% polarization. Radio contours increase by factors of two. Only one polarized jet region is seen, with other regions falling below the detection limit. The greyscale is at far right. See text for details.

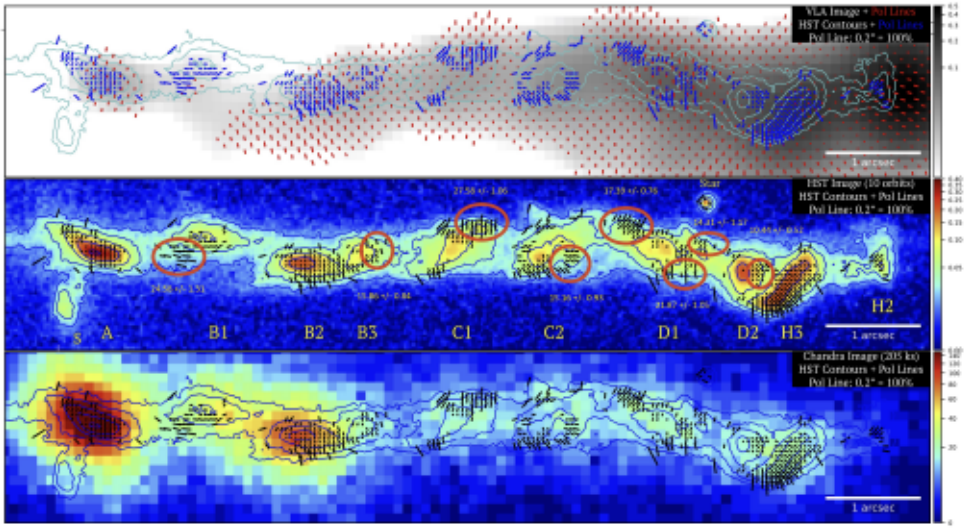

Figure 3. *Top:* VLA 8.4 GHz radio image of the 3C 273 jet (grayscale, scale at right) with radio polarization E-field vectors (in red) and new *HST*/ACS optical Stokes I contours (cyan) + optical polarization vectors (in blue). Optical contours increase by factors of two. *Middle:* Stokes I image using new *HST*/ACS + F606W data (in color, scale at right) with blue contours and black polarization E-field vectors overlaid. Jet components are labeled, and we have circled eight regions that are either at the jet edges or in between knots where the fractional polarization has been measured to be at least as high as that at knot maxima. *Bottom:* Chandra X-ray flux image (in color, scale at right) with *HST*/ACS Stokes I contours overlaid (in blue) and optical polarization E-field vectors (in black). In all cases, a polarization vector is of scale 0.2 arcsec = 100% polarization. We have filtered polarization vectors by showing only pixels with optical polarization SNR > 3.5 and radio polarization SNR > 5.0. Note the strong differences between both optical and radio morphologies in total flux and polarization. The optical flux and morphology is correlated with the X-ray flux in some very interesting ways, as discussed in the text. The color scale for each panel is at the far right.

4. Discussion and Summary

Polarimetry is a powerful diagnostic for jets, and in low-power FR I jets it was critical in addressing fundamental issues, including the 3-dimensional magnetic field configuration and the energetics of the X-ray emission in those jets. In quasar jets, polarimetry can be an equally powerful tool. The highly polarized emissions we observe in these jets cannot be explained by inverse-Comptonized CMB (IC-CMB) emission, which as shown by the synchrotron emission models of PKS 1136–135 [34], requires extremely high Lorentz factors ($\gtrsim 40$) and viewing angles within a few degrees. That was seen to be inconsistent with the observed properties of that source. While some of these sources are known to be highly beamed on parsec scales—for example, 3C 273 has apparent superluminal speeds as high as 15c [39]—it has always been assumed that jets must decelerate on kpc scales (e.g., [42,47], and moreover, in the case of 3C 273, a study of proper motions on the kiloparsec scales found an upper limit of 2c [40], highly inconsistent with the requirement of the IC-CMB model [36,40]. Individually, in fact, those models show that these knots are inconsistent with IC-CMB emission by large factors—anywhere from 2σ for the faintest components to over 20 σ for the brightest components.

If the optical through X-ray emission is due to the IC/CMB process, the optical emission is then linked to heretofore-untracked $\gamma < 10$ electrons, which must provide most of the jet's mass/energy budget. If, as indicated by our observations of PKS 1136–135, the optical through X-ray emission in FR II jets is due to the synchrotron process, that emission would need to emerge from a second electron population [16–19]. But because synchrotron emission at X-ray energies is extremely efficient, the power requirements are modest [13]. More importantly, polarimetry can constrain the co-spatiality of the emission in different energies at scales smaller than can be resolved.

As shown in Figures 1–3, all three of our sources show strongly polarized optical emission in their kiloparsec-scale jets. In all three jets, the X-ray emission appears to be connected to the optical-UV emission via a single spectral component [13,15,16,43,44]. The high polarizations we observe in these sources are not consistent with an IC/CMB emission for the jet X-ray emission, as they would require a very high beaming factor, as was found for PKS 1136–135 by [34]. However, our findings are consistent with synchrotron emission in these jets, with the optical-to-X-ray emission arising in a second, high energy electron population.

In 1150 + 497 and PKS 0637–752, the polarized optical emissions we see come from X-ray and optical knot maxima, similar to what was observed for PKS 1136–135 [34]. However, in the jet of 3C 273, from knots B2 through D the most highly polarized emissions are on the jet edge whereas the knot maxima fall into a low-polarization channel. By comparison, the jet X-ray emission is dominated by discrete knots, with the jet edges being much fainter [15]. While this may seem paradoxical, a similar set of characteristics was noted in some regions of the M87 jet, as well as those of other FR I radio galaxies [5,7–10,23]. The finding that a similar characteristic is seen in one of the nearest optical and X-ray emitting quasar jets, indicates that even at scales of tens to hundreds of kiloparsecs from the active nucleus, particle acceleration can occur both in discrete sites and continuously, by different mechanisms. We will comment further on these findings in a future paper (Clautice et al., 2020, in preparation).

Author Contributions: The concept and methodology for this research was work done by E.S.P., M.C., W.B.S. and S.A. Data reduction, formal analysis and software was work done by D.C. and M.C. investigation was work done by M.G. and E.M. All authors have read and agreed to the published version of the manuscript.

Funding: This research was funded by NASA under STScI grants HSTGO-14696.001-A, HSTGO-13764.001-A and HSTGO-11138.001-A. It was also funded by NSF under grant AST-1715607.

Conflicts of Interest: The authors declare no conflict of interest.

References

1. Rawlings, S.; Saunders, R. Evidence for a common central-engine mechanism in all extragalactic radio sources. *Nature* **1991**, *349*, 138–140. [CrossRef]
2. Fanaroff, B.L.; Riley, J.M. The morphology of extragalactic radio sources of high and low luminosity. *Mon. Not. R. Astron. Soc.* **1974**, *167*, 31P–36P. [CrossRef]
3. Perlman, E.S.; Biretta, J.A.; Sparks, W.B.; Macchetto, F.D.; Leahy, J.P. The Optical-Near-Infrared Spectrum of the M87 Jet fromHubble Space Telescope Observations. *Astrophys. J.* **2001**, *551*, 206–222. [CrossRef]
4. Hardcastle, M.J.; Birkinshaw, M.; Worrall, D.M. Chandra observations of the X-ray jet in 3C 66B. *Mon. Not. R. Astron. Soc.* **2001**, *326*, 1499–1507. [CrossRef]
5. Perlman, E.S.; Wilson, A.S. The X-Ray Emissions from the M87 Jet: Diagnostics and Physical Interpretation. *Astrophys. J.* **2005**, *627*, 140–155. [CrossRef]
6. Perlman, E.S.; Biretta, J.A.; Zhou, F.; Sparks, W.B.; Macchetto, F.D. Optical and Radio Polarimetry of the M87 Jet at 0.2" Resolution. *Astron. J.* **1999**, *117*, 2185–2198. [CrossRef]
7. Perlman, E.S.; Padgett, C.A.; Georganopoulos, M.; Sparks, W.B.; Biretta, J.A.; O'Dea, C.P.; Baum, S.A.; Birkinshaw, M.; Worrall, D.M.; Dulwich, F.; et al. Optical Polarimetry of the Jets of Nearby Radio Galaxies. I. The Data. *Astrophys. J.* **2006**, *651*, 735–748. [CrossRef]
8. Dulwich, F.; Worrall, D.M.; Birkinshaw, M.; Padgett, C.A.; Perlman, E.S. The structure of the jet in 3C 15 from multiband polarimetry. *Mon. Not. R. Astron. Soc.* **2007**, *374*, 1216–1226. [CrossRef]
9. Dulwich, F.; Worrall, D.M.; Birkinshaw, M.; Padgett, C.A.; Perlman, E.S. The magnetic field and geometry of the oblique shock in the jet of 3C 346. *Mon. Not. R. Astron. Soc.* **2009**, *398*, 1207–1216. [CrossRef]
10. Perlman, E.S.; Padgett, C.A.; Georganopoulos, M.; Worrall, D.M.; Kastner, J.H.; Franz, G.; Birkinshaw, M.; Dulwich, F.; O'Dea, C.P.; Baum, S.A.; et al. A Multi-Wavelength Spectral and Polarimetric Study of the Jet of 3C 264. *Astrophys. J.* **2010**, *708*, 171–187. [CrossRef]
11. Sambruna, R.M.; Gambill, J.K.; Maraschi, L.; Tavecchio, F.; Cerutti, R.; Cheung, C.C.; Urry, C.M.; Chartas, G. A Survey of Extended Radio Jets with Chandra and the Hubble Space Telescope. *Astrophys. J.* **2004**, *608*, 698–720. [CrossRef]

12. Schwartz, D.A.; Marshall, H.L.; Lovell, J.E.J.; Piner, B.G.; Tingay, S.J.; Birkinshaw, M.; Chartas, G.; Elvis, M.; Feigelson, E.D.; Ghosh, K.K.; et al. Chandra Discovery of a 100 kiloparsec X-Ray Jet in PKS 0637-752. *Astrophys. J. Lett.* **2000**, *540*, 69–72. [CrossRef]
13. Mehta, K.T.; Georganopoulos, M.; Perlman, E.S.; Padgett, C.A.; Chartas, G. Hubble Space Telescope Observations of the Quasar PKS 0637-752: Equipartition Electron-Proton Jet from the Most Complete Spectral Coverage to Date. *Astrophys. J.* **2009**, *690*, 1706–1714. [CrossRef]
14. Jester, S.; Röser, H.J.; Meisenheimer, K.; Perley, R.; Conway, R. HST optical spectral index map of the jet of 3C 273. *Astronomy Astrophys.* **2001**, *373*, 447–458. [CrossRef]
15. Jester, S.; Harris, D.E.; Marshall, H.L.; Meisenheimer, K. New Chandra Observations of the Jet in 3C 273. I. Softer X-Ray than Radio Spectra and the X-Ray Emission Mechanism. *Astrophys. J.* **2006**, *648*, 900–909. [CrossRef]
16. Jester, S.; Meisenheimer, K.; Martel, A.R.; Perlman, E.S.; Sparks, W.B. Hubble Space Telescope far-ultraviolet imaging of the jet in 3C273: A common emission component from optical to X-rays. *Mon. Not. R. Astron. Soc.* **2007**, *380*, 828–834. [CrossRef]
17. Uchiyama, Y.; Urry, C.M.; Cheung, C.C.; Jester, S.; Van Duyne, J.; Coppi, P.; Sambruna, R.M.; Takahashi, T.; Tavecchio, F.; Maraschi, L. Shedding New Light on the 3C 273 Jet with the Spitzer Space Telescope. *Astrophys. J.* **2006**, *648*, 910–921. [CrossRef]
18. Uchiyama, Y.; Urry, C.M.; Coppi, P.; Van Duyne, J.; Cheung, C.C.; Sambruna, R.M.; Takahashi, T.; Tavecchio, F.; Maraschi, L. An Infrared Study of the Large-Scale Jet in Quasar PKS 1136-135. *Astrophys. J.* **2007**, *661*, 719–727. [CrossRef]
19. Harris, D.E.; Krawczynski, H. X-Ray Emission from Extragalactic Jets. *Ann. Rev. Astronomy Astrophys.* **2006**, *44*, 463–506. [CrossRef]
20. Kataoka, J.; Stawarz, Ł. X-Ray Emission Properties of Large-Scale Jets, Hot Spots, and Lobes in Active Galactic Nuclei. *Astrophys. J.* **2005**, *622*, 797–810. [CrossRef]
21. Georganopoulos, M.; Perlman, E.S.; Kazanas, D.; McEnery, J. Quasar X-Ray Jets: Gamma-Ray Diagnostics of the Synchrotron and Inverse Compton Hypotheses: The Case of 3C 273. *Astrophys. J. Lett.* **2006**, *653*, L5–L8. [CrossRef]
22. Hardcastle, M.J. Testing the beamed inverse-Compton model for jet X-ray emission: Velocity structure and deceleration. *Mon. Not. R. Astron. Soc.* **2006**, *366*, 1465–1474. [CrossRef]
23. Avachat, S.S.; Perlman, E.S.; Adams, S.C.; Cara, M.; Owen, F.; Sparks, W.B.; Georganopoulos, M. Multi-wavelength Polarimetry and Spectral Study of the M87 Jet During 2002-2008. *Astrophys. J.* **2016**, *832*, 3. [CrossRef]
24. Wilson, A.S.; Young, A.J.; Shopbell, P.L. Chandra Observations of Cygnus A: Magnetic Field Strengths in the Hot Spots of a Radio Galaxy. *Astrophys. J. Lett.* **2000**, *544*, L27–L30. [CrossRef]
25. Harris, D.E.; Carilli, C.L.; Perley, R.A. X-ray emission from the radio hotspots of Cygnus A. *Nature* **1994**, *367*, 713–716. [CrossRef]
26. Wilson, A.S.; Young, A.J.; Shopbell, P.L. Chandra X-Ray Observations of Pictor A: High-Energy Cosmic Rays in a Radio Galaxy. *Astrophys. J.* **2001**, *547*, 740–753. [CrossRef]
27. Celotti, A.; Ghisellini, G.; Chiaberge, M. Large-scale jets in active galactic nuclei: Multiwavelength mapping. *Mon. Not. R. Astron. Soc.* **2001**, *321*, L1–L5. [CrossRef]
28. Tavecchio, F.; Maraschi, L.; Sambruna, R.M.; Urry, C.M. The X-Ray Jet of PKS 0637-752: Inverse Compton Radiation from the Cosmic Microwave Background? *Astrophys. J. Lett.* **2000**, *544*, L23–L26. [CrossRef]
29. Georganopoulos, M.; Kazanas, D. Relativistic and Slowing Down: The Flow in the Hot Spots of Powerful Radio Galaxies and Quasars. *Astrophys. J. Lett.* **2003**, *589*, L5–L8. [CrossRef]
30. Georganopoulos, M.; Kazanas, D.; Perlman, E.; Stecker, F.W. Bulk Comptonization of the Cosmic Microwave Background by Extragalactic Jets as a Probe of Their Matter Content. *Astrophys. J.* **2005**, *625*, 656–666. [CrossRef]
31. Begelman, M.C.; Sikora, M.; Giommi, P.; Barr, P.; Garilli, B.; Gioia, I.M.; Maccacaro, T.; Maccagni, D.; Schild, R.E. Inverse Compton Scattering of Ambient Radiation by a Cold Relativistic Jet: A Source of Beamed, Polarized X-Ray and Optical Observations of X-Ray–selected BL Lacertae Objects. *Astrophys. J.* **1987**, *322*, 650. [CrossRef]
32. Krawczynski, H. The Polarization Properties of Inverse Compton Emission and Implications for Blazar Observations with the GEMS X-Ray Polarimeter. *Astrophys. J.* **2012**, *744*, 30. [CrossRef]

33. McNamara, A.L.; Kuncic, Z.; Wu, K. X-ray polarization in relativistic jets. *Mon. Not. R. Astron. Soc.* **2009**, *395*, 1507–1514. [CrossRef]
34. Cara, M.; Perlman, E.S.; Uchiyama, Y.; Cheung, C.C.; Coppi, P.S.; Georganopoulos, M.; Worrall, D.M.; Birkinshaw, M.; Sparks, W.B.; Marshall, H.L.; et al. Polarimetry and the High-energy Emission Mechanisms in Quasar Jets: The Case of PKS 1136-135. *Astrophys. J.* **2013**, *773*, 186. [CrossRef]
35. Meyer, E.T.; Georganopoulos, M. Fermi Rules Out the Inverse Compton/CMB Model for the Large-scale Jet X-Ray Emission of 3C 273. *Astrophys. J. Lett.* **2014**, *780*, L27. [CrossRef]
36. Meyer, E.T.; Georganopoulos, M.; Sparks, W.B.; Godfrey, L.; Lovell, J.E.J.; Perlman, E. Ruling out IC/CMB X-rays in PKS 0637-752 and the Implications for TeV Emission from Large-scale Quasar Jets. *Astrophys. J.* **2015**, *805*, 154. [CrossRef]
37. Meyer, E.T.; Breiding, P.; Georganopoulos, M.; Oteo, I.; Zwaan, M.A.; Laing, R.; Godfrey, L.; Ivison, R.J. New ALMA and Fermi/LAT Observations of the Large-scale Jet of PKS 0637-752 Strengthen the Case Against the IC/CMB Model. *Astrophys. J. Lett.* **2017**, *835*, L35. [CrossRef]
38. Breiding, P.; Meyer, E.T.; Georganopoulos, M.; Keenan, M.E.; DeNigris, N.S.; Hewitt, J. Fermi Non-detections of Four X-Ray Jet Sources and Implications for the IC/CMB Mechanism. *Astrophys. J.* **2017**, *849*, 95. [CrossRef]
39. Lister, M.L.; Homan, D.C.; Hovatta, T.; Kellermann, K.I.; Kiehlmann, S.; Kovalev, Y.Y.; Max-Moerbeck, W.; Pushkarev, A.B.; Readhead, A.C.S.; Ros, E.; et al. MOJAVE. XVII. Jet Kinematics and Parent Population Properties of Relativistically Beamed Radio-loud Blazars. *Astrophys. J.* **2019**, *874*, 43. [CrossRef]
40. Meyer, E.T.; Sparks, W.B.; Georganopoulos, M.; Anderson, J.; van der Marel, R.; Biretta, J.; Sohn, S.T.; Chiaberge, M.; Perlman, E.; Norman, C. An HST Proper-motion Study of the Large-scale Jet of 3C273. *Astrophys. J.* **2016**, *818*, 195. [CrossRef]
41. Edwards, P.G.; Piner, B.G.; Tingay, S.J.; Lovell, J.E.J.; Kataoka, J.; Ojha, R.; Murata, Y. The Parsec-Scale Jet of PKS 0637-752. *Publ. Soc. Jpn.* **2006**, *58*, 233–241. [CrossRef]
42. Worrall, D.M. The X-ray jets of active galaxies. *Astron. Astrophys. Rev.* **2009**, *17*, 1–46. [CrossRef]
43. Sambruna, R.M.; Gliozzi, M.; Donato, D.; Maraschi, L.; Tavecchio, F.; Cheung, C.C.; Urry, C.M.; Wardle, J.F.C. Deep Chandra and Multicolor HST Follow-up of the Jets in Two Powerful Radio Quasars. *Astrophys. J.* **2006**, *641*, 717–731. [CrossRef]
44. Jester, S.; Röser, H.J.; Meisenheimer, K.; Perley, R. X-rays from the jet in <ASTROBJ>3C 273</ASTROBJ>: Clues from the radio-optical spectra. *Astronomy Astrophys.* **2002**, *385*, L27–L30. [CrossRef]
45. Lovell, J.E.J.; Tingay, S.J.; Piner, B.G.; Jauncey, D.L.; Preston, R.A.; Murphy, D.W.; McCulloch, P.M.; Costa, M.E.; Nicolson, G.; Hirabayashi, H.; et al. VSOP and ATCA Observations of PKS 0637-752. In *Astrophysical Phenomena Revealed by Space VLBI*; Hirabayashi, H., Edwards, P.G., Murphy, D.W., Eds.; 2000; pp. 215–218.
46. Perley, R.A.; Meisenheimer, K. High-fidelity VLA imaging of the radio structure of 3C 273. *Astronomy Astrophys.* **2017**, *601*, A35. [CrossRef]
47. Blandford, R.; Meier, D.; Readhead, A. Relativistic Jets from Active Galactic Nuclei. *Ann. Rev. Astronomy Astrophys.* **2019**, *57*, 467–509. [CrossRef]